Nuclear Engineering and Technology 53 (2021) 3517–3527

Contents lists available at ScienceDirect

Nuclear Engineering and Technology

journal homepage: www.elsevier.com/locate/net

Original Article

An ultra-long-life small safe fast reactor core concept having heterogeneous driver-blanket fuel assemblies

Kyu Jung Choi [a], Yeonguk Jo [b], Ser Gi Hong [a, *]

[a] Department of Nuclear Engineering, Hanyang University, 222 Wangsimni-ro, Seongdong-gu, Seoul, 04763, South Korea
[b] Department of Nuclear Engineering, Kyung Hee University, 1732 Deogyeong-daero, Giheung-gu, Yongin-si, Gyeonggi-do, 17104, South Korea

ARTICLE INFO

Article history:
Received 17 August 2020
Received in revised form
7 May 2021
Accepted 9 May 2021
Available online 15 May 2021

Keywords:
Ultra-long-life small fast reactor
Heterogeneous assemblies
Sodium void worth
Monte Carlo depletion

ABSTRACT

New 80-MW (electric) ultra-long-life sodium cooled fast reactor core having inherent safety characteristics is designed with heterogeneous fuel assemblies comprised of driver and blanket fuel rods. Several options using upper sodium plenum and SSFZ (Special Sodium Flowing Zone) for reducing sodium void reactivity are neutronically analyzed in this core concept in order to improve the inherent safety of the core. The SSFZ allowing the coolant flow from the peripheral fuel assemblies increases the neutron leakage under coolant expansion or voiding. The Monte Carlo calculations were used to design the cores and analyze their physics characteristics with heterogeneous models. The results of the design and analyses show that the final core design option has a small burnup reactivity swing of 618 pcm over ~54 EFPYs cycle length and a very small sodium void worth of ~35pcm at EOC (End of Cycle), which leads to the satisfaction of all the conditions for inherent safety with large margin based on the quasi-static reactivity balance analysis under ATWS (Anticipated Transient Without Scram).
© 2021 Korean Nuclear Society, Published by Elsevier Korea LLC. This is an open access article under the CC BY-NC-ND license (http://creativecommons.org/licenses/by-nc-nd/4.0/).

1. Introduction

The commercial nuclear power reactors such as PWR, BWR, and CANDUs have economically and steadily supplied electricity for many countries. However, they have limitations on the utilization of uranium resources and generate a large number of spent fuels, which are resulted from the once-through fuel cycle and low discharge burnup even if many PWRs in France were authorized to load MOX fuels and successfully used MOX fuels in ~22 PWRs of 900 MWe [1]. On the other hand, fast reactors such as SFR (Sodium cooled Fast Reactor) and LFR (Lead cooled Fast Reactor) have been considered as a promising option for long-term sustainable energy production with high uranium utilization and with recycling of actinides due to their fast neutron spectra and superior neutron economy such as high fission-to-capture ratio and the larger number of neutrons released per fission [2–4]. In particular, the recycling of actinides and breeding in fast spectrum reactors drastically reduce the amount of spent fuel going to the geological repository and drastically improves the uranium utilization [3,5]. Spent fuels from PWRs can be reprocessed, and plutonium or TRU (Transuranics) can be recycled in PWRs. However, the number of recycling is limited due to several technical issues such as difficulties in the fuel fabrication and degradations of core physics parameters [6,7].

On the other hand, the recycling of actinides requires an advanced reprocessing technique with remote processing, and it can be involved with the proliferation issues. Recently, the ultra-long-life fast reactors, which can be operated over several tens of years without refueling, have been actively studied in the world. There have been several different types of ultra-long-life cores, such as CANDLE [8,9] and the initial version of TWR (Traveling Wave Reactor) [10–15]. In these reactors, the initial fission power is generated in small driver fuel regions containing enriched uranium or PWR spent fuel TRU (Transuranics), and then the neutrons generated by the driver fuel move into the large blanket regions of depleted uranium in which the neutrons breed the fissile nuclides. So, there is a slow propagation of the burning region and fission power distribution. For these reactors, a very high burnup larger than 120 MWd/kg can be achieved with long cycle operation over several tens of years without refueling. Another type of reactor having high discharge burnup is known as the “Standing Wave (SW) Variant” of TWR, which was suggested by TerraPower [10,12,16,17]. This type of reactor utilizes a large number of fuel batches and periodic refueling over 1–2 EFPYs. The unique feature

* Corresponding author.
E-mail address: hongsergi@hanyang.ac.kr (S.G. Hong).

https://doi.org/10.1016/j.net.2021.05.013
1738-5733/© 2021 Korean Nuclear Society, Published by Elsevier Korea LLC. This is an open access article under the CC BY-NC-ND license (http://creativecommons.org/licenses/by-nc-nd/4.0/).

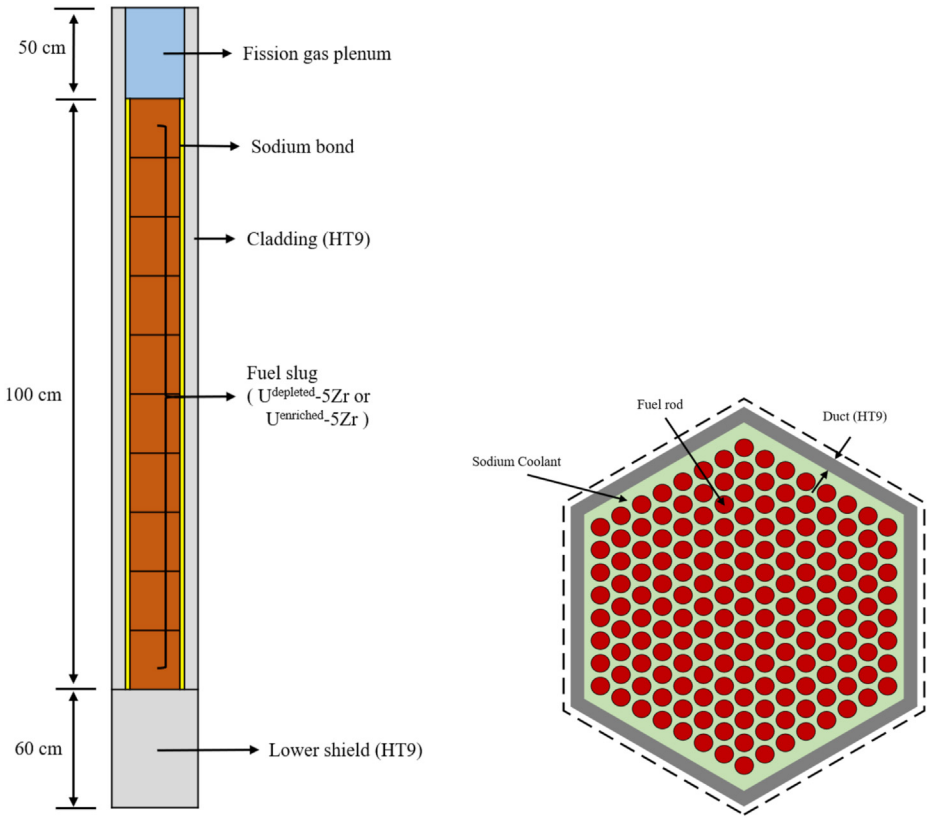

Fig. 1. Configuration of the fuel rod and assembly.

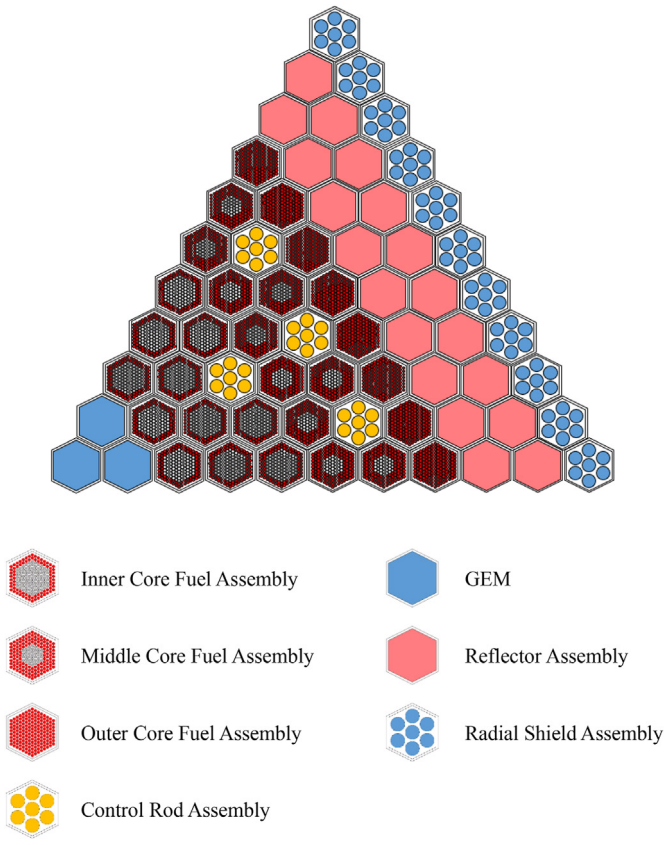

Fig. 2. Radial configurations of the reference core (Design I, one-sixth).

of this type of reactors is the fact that depleted or natural uraniums are only supplied as the fresh batch fuel due to the full utilization of breed-and-burn characteristics. The TWR and its SW variant can achieve very high burnup and higher uranium utilization up to 30 times than PWRs. On the other hand, these reactors can have high power peaking, and high sodium void reactivity due to the fact that the high burnup region is located in the innermost region and the burnup is very high.

The purpose of this work is to suggest a new concept core having ultra-long-cycle and distinct features (e.g., inherent safety and almost zero sodium void worth) with a heterogeneous assembly concept and to show its neutronic feasibility. The suggested ultra-long-life small SFR cores rate 80 MWe (222 MWt) electricity output and can be operated over ~54 EFPYs without refueling and with low sodium void worth [18–20]. This ultra-long-life SFR core employs heterogeneous fuel assemblies in addition to the homogeneous ones. The heterogeneous fuel assemblies are comprised of the driver (enriched uranium) and the blanket (depleted uranium) fuel rods. They are devised to achieve ultra-long-life and to minimize the propagation of the power distribution by allowing the power propagation within the heterogeneous fuel assemblies. The homogeneous driver fuel assemblies are located only in the outer region, which drives initial fissions, while the heterogeneous assemblies having blanket and driver rods are in the inner and middle regions. Also, we introduced GEM (Gas Expansion Module)s and SSFZ (Special Sodium Flowing Zone) for improving inherent safety of the core. In particular, SSFZ in the peripheral region of the active core is introduced to reduce sodium void worth by increasing radial neutron leakage under sodium voiding. The analysis results show that the final core has 54 EFPYs cycle length, almost zero sodium void worth of ~35 pcm even at EOC, and very low burnup reactivity swing, which led to the full satisfaction with large margins of all the

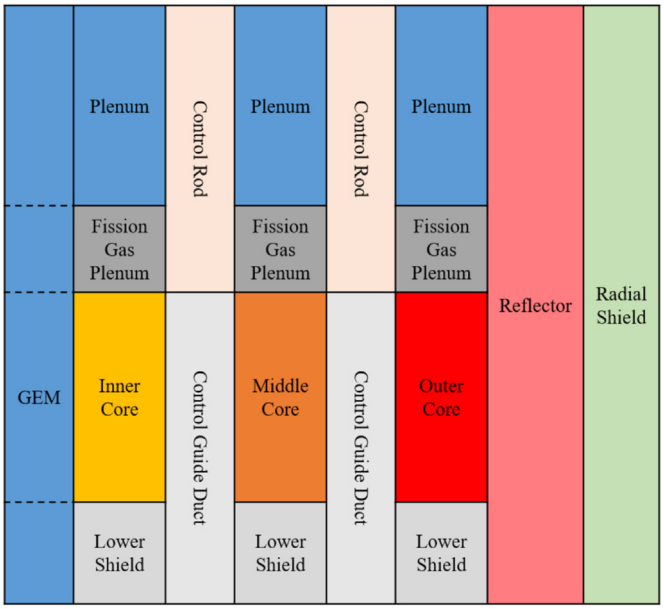

Fig. 3. Axial core configuration of the reference core.

Table 1
Comparison of the design parameters of the reference core.

Design parameter	Values
Reactor power (MWe/MWt)	80/222
Fuel rod diameter (cm)	1.4
Cladding thickness (mm)	0.55
Duct thickness (mm)	3.7
Lattice pitch (cm)	1.55
Pitch-to-diameter ratio	1.11
Assembly pitch (cm)	21.53
Fuel type (Driver/Blanket)	U–5Zr/DU-5Zr
Fuel density (g/cm^3)	17.3
Active Core volume (m^3)	5.54
Average linear power density (W/cm)	95.2
Average power density (W/cm^3)	40.1
Average specific power (W/g)	5.9
Volume fractions (%) per assembly	
Fuel/coolant/structure	56.5/16.9/26.5
Actinide inventory (kg) in driver fuels	27,678
Actinide inventory (kg) in blanket fuels	9899
Number of fuel rods/FA	
Driver	[a]78/132/169
Blanket	[a]91/37/0

[a] Inner core/middle core/outer core.

conditions for inherent safety based on the quasi-static reactivity balance analysis.

In Section 2, the computational methods for designing and analyzing the cores are described. Section 3 describes the designs of the suggested cores and the results of the analyses for the cores. Finally, the summary and conclusions are given in Section 4.

2. Calculation method for core design and analysis

The core neutronic calculations, including fuel depletion, were performed using MCNP6 [21] developed by LANL and Serpent [22] developed by VTT. In particular, the geometric modeling using these Monte Carlo codes was performed with explicitly heterogeneous representations down to fuel slug, cladding, and fuel assembly ducts so as to accurately consider the heterogeneous effects that would be resulted from the use of heterogeneous fuel assemblies. The ENDF/B-VII.r0 point-wise cross section library was used for all the depletion calculations and core physics parameter evaluations. MCNP6 was used in the initial stages of the core design for exploring the design options but the MCNP6 calculations including depletion calculations take lots of computing time, which makes it difficult to perform the design optimization with parametric studies. So, we set up the Serpent code which was used to the calculations in finalizing the core design (i.e., Serpent was used in Sec. 3.2.2).

For the initial depletion analysis using MCNP6 (in Sec. 3.1 and in Sec. 3.2.1), the core was divided into three radial zones (i.e., inner, middle, and outer zones), and each of them is sub-divided into the driver and blanket zones (i.e., driver and blanket fuels are grouped into the driver and blanket zones, respectively). So, the number of radial zones for depletion is five. Furthermore, these depletion zones are axially divided into five sub-zones, which leads to a total 25 depletion zones. On the other hand, the optimization study (in Sec. 3.2.2) was performed with radially more refined zoning in which each assembly is treated as a zone with separate zones of blanket and driver each. So, the total number of radial zones is 26 with one-sixth symmetry of the core, and the total number of depletion zones is 130 (i.e., 26 radial zones x 5 axial zones). The accuracy of this depletion zoning is checked with a comparison with a more refined axial zoning and a large number of histories in Sec. 3.2.2. On the other hand, the depletion time step size is set to one year which corresponds to ~2.15 MWd/kg. The results obtained using a depletion time step size of one year are compared with the results using 0.5 years depletion time step. The numbers of active and inactive cycles, and the number of histories per each cycle for Monte Carlo transport calculations using MCNP6 were determined to give a small standard deviation on the k_{eff} less than 60 pcm for depletion calculations (i.e., 20 inactive and 120 active cycles with each 5000 histories) while they are determined to give much small standard deviation on the k_{eff} less than 6 pcm standard deviation for core physics parameter evaluations (i.e., 50 inactive and 500 active cycles with each 10,000 histories). On the other hand, the depletion calculations using Serpent were performed using 100 inactive and 1100 active cycles with each 100,000 histories giving

Table 2
Comparison of the performance parameters of the reference core.

Parameter	Values
Fuel type	U–5Zr
Cycle length (EFPYs)	76
Initial uranium enrichment (wt%)	
Driver/Blanket	14.75/Depleted U (0.2 wt%^{235}U)
Burnup reactivity swing (pcm)	1590
Fuel burnup (MWd/kg)	
Inner core (Driver/Blanket)	203/117
Middle core (Driver/Blanket)	195/111
Outer core (Driver/Blanket)	159/NA
Total core	162
Sodium void worth (pcm, BOC/EOC)	−427/1518
Reactivity coefficients (pcm/K, BOC/EOC)	
Doppler (900 K)	−0.436/−0.220
Fuel axial expansion	−0.222/−0.247
Core support radial expansion	−0.823/−1.182
Coolant expansion	−0.0084/0.5440
Effective delayed neutron fraction (β_{eff}, BOC/EOC)	0.00706/0.00381
Pu content in driver fuel (wt%, EOC)	
Inner/middle/outer	9.86/9.41/8.05
Pu content in blanket fuel (wt%, EOC)	
Inner/middle/outer	10.01/9.62/NA
TRU content in driver fuel (wt%, EOC)	
Inner/middle/outer	10.34/9.84/8.38
TRU content in blanket fuel (wt%, EOC)	
Inner/middle/outer	10.15/9.76/NA

small statistical errors less than 10 pcm while 100 inactive and 1500 active cycles with each 168,000 histories were used for core physics parameter evaluations to give small standard deviation less than 4 pcm.

3. Core design and analysis

3.1. Reference core design

We targeted a small sodium cooled fast reactor core rather than the medium or large ones to achieve negative or small positive sodium void reactivity while an ultra-long-life operation and a small burnup reactivity swing less than 2000 pcm over ~50 EFPYs were considered as the main design goals. The discharge burnup higher than ~120 MWd/kg is also an important design goal to achieve high fuel economy. High breeding is required to satisfy these design goals, and a hard neutron spectrum is needed to achieve high breeding. The metallic fuel is desirable for this purpose due to its high heavy metal density and high mass numbers of its constituent nuclides [23]. We considered the binary metallic fuel of U–5Zr with a typical smear density of 75%. The fuel slug of U–5Zr is enclosed by a sodium bond region which fills the annular region between the fuel slug and 0.55 mm thick HT9 cladding. The composition of HT9 is 87.19% Fe, 9.94% Cr, 1.27% Mo, 0.49% Ni, 0.48% Mn, 0.20% C, 0.19% V, and 0.08% Si. Fig. 1 shows the configurations of the fuel rods and fuel assemblies. The bottom region below the fuel is a 60 cm thick lower shield made of HT9 and a 50 cm thick fission gas plenum above the active fuel is considered to reduce fission gas pressure, but we implicitly assumed some ventilation pass of the fission gases through the sodium plenum region or lower fuel region due to its short fission gas plenum and long-life operation.

The thermal output of the core is 222 MWt, and a low linear heat generation rate of 95.2 W/cm is selected to achieve ultra-long-life operation. The short active core height of 100 cm is considered to achieve small sodium void reactivity. As mentioned in Section 1, a unique feature of this small SFR core is the use of the heterogeneous fuel assemblies comprised of driver and blanket fuel rods. For each assembly, 169 fuel rods are closely packed with the typical triangular pitch lattice in a 3.7 mm thick hexagonal duct. These heterogeneous fuel assemblies are devised to mitigate the propagation of the power distribution by allowing the power propagation within the heterogeneous fuel assemblies and to control burnup reactivity swing. The driver and blanket fuels use enriched and depleted uranium, respectively. Fig. 2 shows the configuration of the fuel assemblies and the reference core (Design I).

As shown in Fig. 2, the core has seven central GEMs (Gas Expansion Module) (denoted by blue color in Fig. 2), which are sequentially followed by the inner, middle, and outer fuel regions. GEM is a 3.7 mm thick duct where an argon gas bubble trapped expands with the core inlet pressure decrease and expels the sodium inside it. The GEM technology was considered to insert negative reactivity during the primary system loss of flow. The fuel regions are surrounded by two rings of the reflector assemblies followed by one ring of the shield assemblies. The active core is divided into three regions. Each fuel assembly in three core regions has different numbers of driver and blanket fuel rods to control depletion behavior and power distribution. The reflector assemblies are the ducts filled with lead, which were considered to reduce radial neutron leakage due to the high scattering cross section of lead. In addition, these lead-filled reflectors also can play a role as a gamma shield. As shown in Fig. 2, the control rod assembly consists of seven absorber rods. In each absorber rod, the B_4C (55 wt% B-10 enrichment) absorber is enclosed by a 0.2 cm thick HT9 cladding of 6.0 cm inner diameter. There are 24 control rod assemblies in the core. At present, the control rod assemblies have not been optimized with practical considerations, but we checked that the control assemblies have a large reactivity worth of ~26.9% $\Delta\rho$. The radial shield assembly also consists of seven rods, but each rod is composed of HT9, and its outer diameter is 3.58 cm. The axial configuration of the cores is shown in Fig. 3. The region above the fission gas plenum is the sodium plenum region assumed to be 150 cm. Practically, the sodium plenum region contains some structural materials, but we did not consider the structural materials in the sodium plenum region due to its small fraction and minor effect on reactivity (e.g., 92% sodium and 8% steel) [24].

The main design parameters of these cores are specified in Table 1. As shown in Table 1, these cores employ the thick fuel rods having 1.4 cm outer diameter and a tight lattice structure having a pitch-to-diameter ratio of 1.11 to achieve a high fuel volume fraction (i.e., 56.5 $^{v}/_{o}$) including the bond region between fuel slug and cladding to meet the ultra-long-life operation. As mentioned before, the core has low linear and volumetric power densities of 95.2 W/cm and 40.1 W/cm^3, respectively, which lead to a low specific power of 5.9 W/g. The small coolant volume fraction due to its tight lattice structure can be led to degradation of cooling capability (e.g., large pressure drop resulted from large friction loss) but the low power density would mitigate this issue even if a detailed thermal analysis was not performed. This level of specific power is similar to those of the previous ultra-long-life cores [25,26]. Each fuel assembly of the inner core comprises 78 driver and 91 blanket rods while the one in the middle core comprises 132 driver and 37 blanket rods, and the outer core assembly (i.e., 8th ring assemblies) comprises only driver rods. In the heterogeneous fuel assemblies, it should be noted that the driver rods are arranged in the outer region enclosing inner blanket rods in order to increase initial reactivity by making the driver rods neighboring together.

The main core physics parameters are summarized in Table 2. The initial uranium enrichments are determined such that the

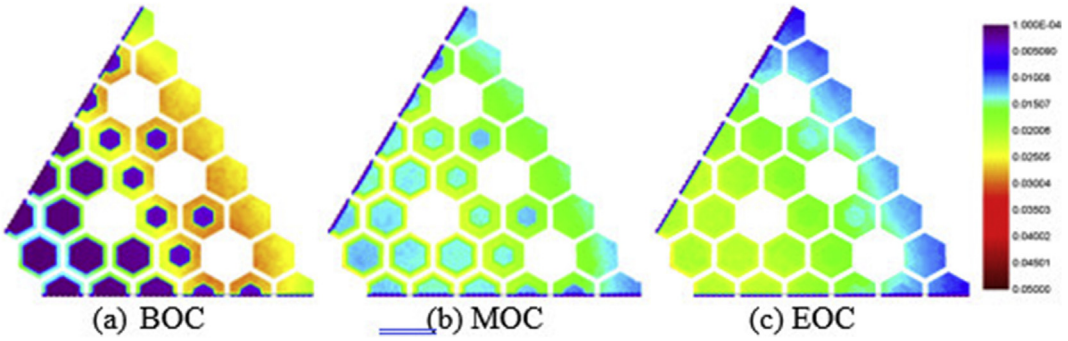

Fig. 4. Comparison of the pin-wise power distributions (arbitrary unit) of the reference core at BOC, MOC, and EOC.

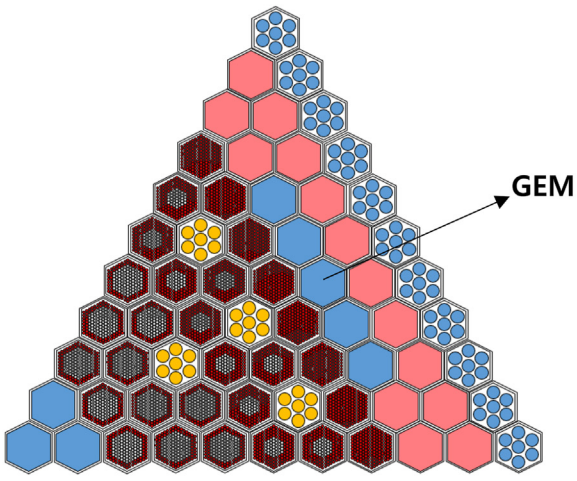

(a) Radial configuration

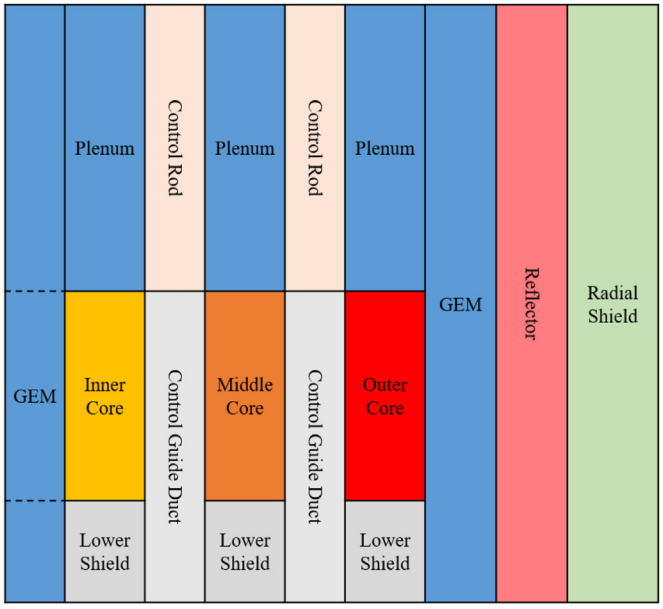

(b) Axial configuration

Fig. 5. Radial and axial configuration of Design I–B core.

initial k_{eff} is to be ~1.003. An extra reactivity of ~300 pcm from criticality was taken to consider uncertainties in criticality calculation. The reference core has an initial uranium enrichment of 14.75 wt% and a burnup reactivity swing of 1590 pcm over its cycle length of 76 EFPYs (Please see Fig. 6 for the evolution of k_{eff} over depletion time). The core has a negative sodium void worth of −427 pcm at BOC, while it has a considerably positive sodium void worth of 1518 pcm at EOC. The initially negative sodium void worth at BOC comes from the fact that the fission reactions mostly occur by ^{235}U in the outer driver region and the sodium voiding leads to the significant capture rate in the blanket (i.e., ^{238}U) and to increase radial neutron leakage through outer core boundary. On the other hand, large positive sodium void worth at EOC has resulted from the fact that the fission reactions are mainly occurred from TRUs having increasing η values by sodium voiding and that radial neutron leakage under sodium voiding is reduced in comparison with that at BOC due to the power distribution shift into inner region.

The outer core driver fuels reach a high burnup of 159 MWd/kg, and the blanket fuels of the inner and middle cores also have high burnup of 117 and 111 MWd/kg, respectively. As expected, the reference core has all negative temperature reactivity coefficients at BOC while it has small positive temperature reactivity coefficients by coolant expansion at EOC. The Doppler coefficient was calculated by changing the fuel temperature by 100 °C while the reactivity coefficients by axial fuel expansion and radial expansion of core support structure were by assuming 10% expansions of active fuel length and lattice pitch, respectively. The reactivity coefficient by coolant expansion was calculated using 10% change in the density of the flowing sodium coolant. The calculated reactivity changes were divided by the temperature changes corresponding to the expansions. For sodium void worth calculation, we considered voiding only for the flowing sodium coolants, and we did not consider the voiding of sodium in the gap region among the fuel assembly ducts.

The TRU and plutonium contents both in driver and blanket fuels are analyzed at EOC, and they are also summarized in Table 2. As expected, a high burnup leads to higher TRU and plutonium contents. It is noted that the blanket fuels have higher plutonium contents than the driver ones.

Fig. 4 compares the pin-wise fission power distributions (arbitrary unit) of the reference core at BOC, MOC, and EOC. This figure shows that the propagations of the power from driver to blanket occur in the fuel assembly level even if there is also a broad power propagation from outer and middle regions to inner one. The fission power is initially distributed over the driver rods of the middle and outer core regions while the power distribution at MOC is well spread out over all the driver rods and partially smeared into the blanket rods, and then it propagates into all the fuel rods at EOC.

3.2. Alternative core designs for reducing sodium void worth

3.2.1. Consideration of upper sodium plenum and outer GEMs

In this section, alternative core design options are suggested and analyzed in order to further reduce sodium void worth and reactivity coefficient by coolant expansion which are the main parameters negatively affecting the inherent safety. For this purpose, we first considered the upper sodium plenum above the active fuel, and the height of the upper sodium plenum was assumed to be 200 cm in the calculations, although this requires some technical consideration such as an advanced ventilation system of fission gas or lower fission gas plenum [27]. There have also been other studies to reduce sodium void worth with upper sodium plenum in the different types of sodium-cooled fast reactors that are not ultra-long-cycle cores [24,28,29]. This alternative design core having the same loading pattern as the Design I core is designated as Design I-A. Also, we replaced a part of the reflector region with 30 GEMs to effectively increase neutron leakage under the loss of the primary coolant loss. This alternative core design with upper sodium plenum and GEMs is designated as Design I–B. Fig. 5 shows the radial and axial configurations of Design I–B core. The evolutions of k_{eff} values for Design I, Design I-A (Design I with upper sodium plenum), and Design I–B (Design I-A with GEMs in reflector region) cores are compared in Fig. 6.

As shown in Fig. 6, the evolution of k_{eff} for Design I-A is similar to that of Design I, which means replacing the upper fission gas plenum with the upper sodium plenum has only a minor effect on the core reactivity. On the other hand, the GEMs in the outer reflector zone (i.e., Design I–B) considerably reduce the cycle length down to 67 EFPYs due to the increases in radial neutron leakage and absorption by sodium in GEMs than lead in the

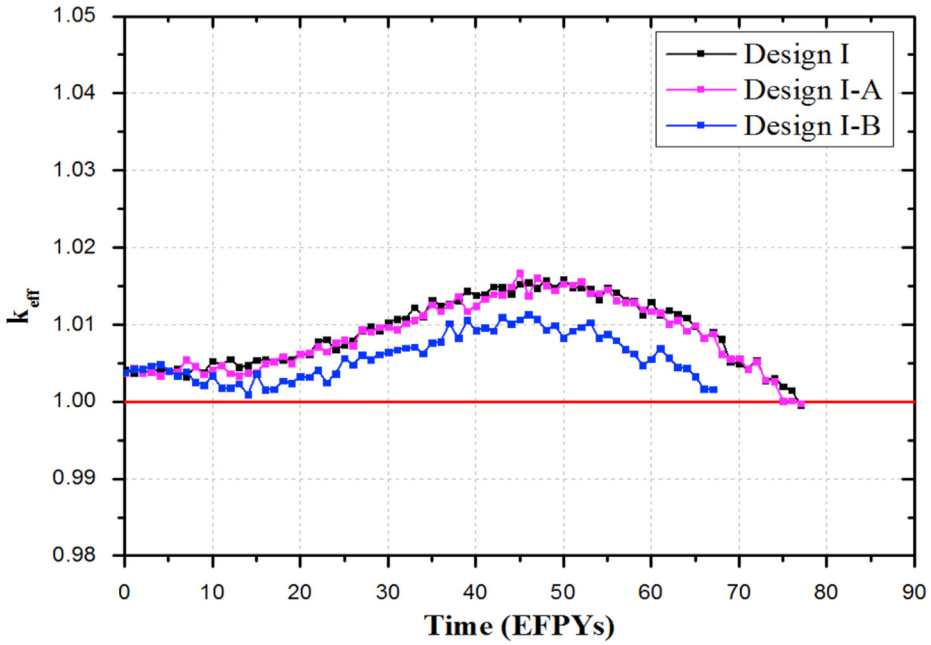

Fig. 6. Comparison of evolutions of k_{eff} for Design I, Design I-A, and Design I–B cores.

Table 3
Comparison of the main performances of the alternative cores.

Parameters	Design I	Design I-A	Design I–B
Cycle length (EFPYs)	76	76	67
Burnup reactivity swing (pcm)	1590	1590	1181
Initial U enrichment (wt%)	14.75	14.75	15.32
Actinide inventories (kg, driver/blanket)	27,678/9899	27,678/9899	29,132/10,419
Fuel burnup (MWd/kg)			
Inner core (driver/blanket)	203/117	202/117	184/98
Middle core (driver/blanket)	195/111	195/111	175/91
Outer core (driver)	159	159	139
Total core	162	162	144
Sodium void worth (pcm, BOC/EOC)			
Active core	467/2171	450/2176	365/2000
Active core + sodium plenum (or gas plenum)	−427/1518	−880/1130	−948/883
GEMs only (pcm, BOC/EOC)	NA	NA	−1643/−430
Effective delayed neutron fraction (β_{eff})	0.00706/0.00381	0.00718/0.00417	0.00665/0.00414
Pu content in driver fuel (wt%, EOC)			
Inner/middle/outer	9.86/9.41/8.05	9.87/9.40/8.05	9.09/8.55/7.08
Pu content in blanket fuel (wt%, EOC)			
Inner/middle/outer	10.01/9.62/0	10.01/9.61/0	9.34/8.85/0
TRU content in driver fuel (wt%, EOC)			
Inner/middle/outer	10.34/9.84/8.38	10.34/9.84/8.38	9.51/8.92/7.36
TRU content in blanket fuel (wt%, EOC)			
Inner/middle/outer	10.15/9.76/0	10.15/9.75/0	9.46/8.97/0

Note: All values in this table are calculated with MCNP6.

reflector assemblies. Table 3 compares the core performance parameters of these cores. The initial uranium for Design I–B is slightly increased to be 15.32 wt%. In comparison with Design I, the Design I-A core has almost the same sodium void worth only for active core sodium voiding as the reference core, but it has considerably reduced sodium void worths by 453 pcm and 388 pcm at BOC and EOC, respectively, for sodium voiding both in active core and the upper gas plenum. These reduced sodium void worths are mainly due to the axial neutron leakage increase through the upper sodium plenum under sodium voiding.

The Design I–B core having GEMs in the reflector region has a smaller burnup reactivity swing by 409 pcm over 67 EFPYs cycle length than the reference core (i.e., Design I), which reduces the reactivity requirement of the control rod assemblies. On the other hand, this core has reduced fuel burnups due to the shorter cycle length, but its blanket burnups are still considerable (>90 MWd/kg). This core has a smaller sodium void worth by 68 pcm and 247 pcm at BOC and EOC, respectively, than Design I-A for sodium voiding both in the active core and the gas plenum. It is considered that these smaller sodium void worth of Design I–B are resulted from the large radial neutron leakage and smaller burnup than Design I-A. Also, it is noted in Table 3 that the sodium level decreases down to the bottom of the active core in GEMs leads to negative reactivity of −1643 and −430 pcm at BOC and EOC, respectively.

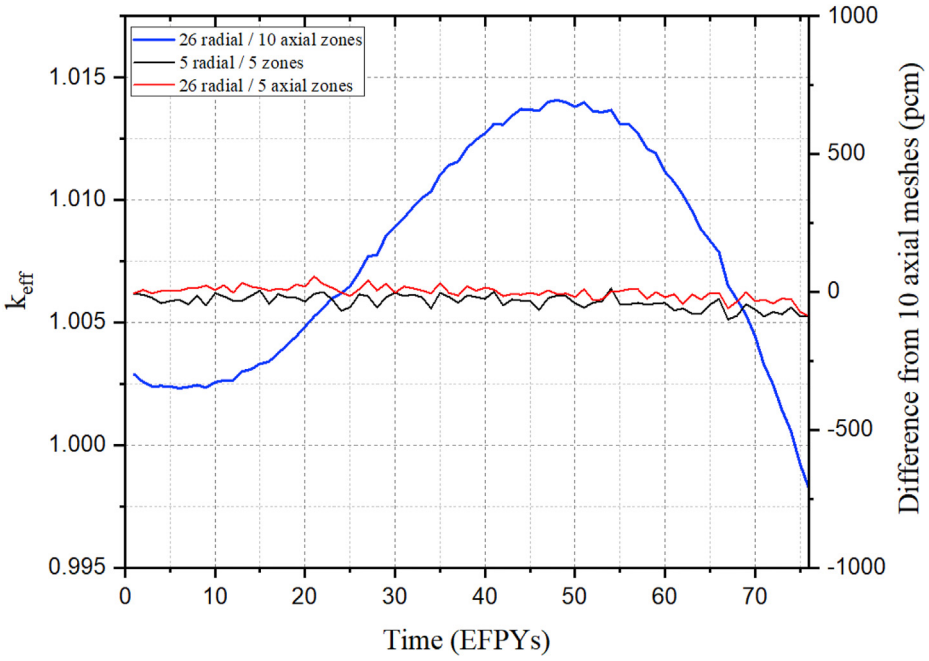

Fig. 7. Comparison of k_{eff} discrepancies for different depletion zonings from the most refined zoning of 26 radial and 10 axial zones having 100 inactive and 1100 active cycles with 100,000 histories per cycle (depletion time step: 0.5 years).

3.2.2. Determination of final candidate

In this subsection, we tried to find a better core design having further reduced sodium void worth. Before going to this design optimization, the depletion calculation accuracy was assessed by considering various different divisions of the depletion zone. As described in Sec. 2, the calculations given in the previous sections were performed with 5 radial and 5 axial zones (total 25 depletion zones) where the core is divided into three radial zones (inner, middle, and outer ones) and the driver and blanket fuel rods are divided into each zone. We considered two more refined zonings than the reference case. In the first refined zoning, each assembly is treated as a zone with separate subzones of driver and blanket fuel rods each. So, the total number of radial depletion zones is 26 with one-sixth symmetry of the core, and the total number of depletion zones is 130 (i.e., 26 radial zones x 5 axial zones). The second refined zoning considered 10 axial zones. For this zoning case, we used a large number of histories for Monte Carlo depletion calculation and a fine depletion time step size of 0.5 years. This large number of histories (i.e., 100 inactive and 1100 active cycles with 100,000 histories per each cycle) are considered to reduce the propagation of statistical uncertainties in reaction rates that would be resulted from refined zoning. The standard deviations of k_{eff} during depletion with these histories and cycles were shown to be less than 6 pcm. The reactivity change as depletion obtained with this most refined depletion zoning was used as the reference results. In this subsection, we used Serpent Monte Carlo code to reduce computing time because the Monte Carlo transport calculations using heterogeneous assembly models require a large amount of computing cost when it is coupled with depletion calculations.

Fig. 7 compares the discrepancies of k_{eff} values from the most refined zoning (i.e., 26 radial zones and 10 axial zones) for the considered different depletion zonings. From this figure, it is shown that the initial depletion zoning with 5 radial and 5 axial zones has discrepancies in k_{eff} less than 100 pcm. In comparison, the more refined one with 26 radial and 5 axial zones has discrepancies in k_{eff} less than 60 pcm. This analysis result shows that two considered zonings for depletion have reasonable accuracy compared to the most refined depletion zoning case using a large number of histories for Monte Carlo transport simulation. The depletion analysis for the final core was performed with 26 radial and 5 axial depletion zones (i.e., totally 130 depletion zones) using 100 inactive and 1100 active cycles with 100,000 histories per each cycle, and using one year as the depletion time step.

Also, we considered 8% axial fuel swelling and changed HT9-based radial shield assemblies to the ones based B_4C absorber by reflecting the comments during the review process in analyzing the final core. The radial shield assembly consists of seven B_4C rods. The inner and outer radii of each B_4C rod are 3.2 cm and 3.7 cm, respectively and the material of cladding is HT9. Natural boron was used in the B_4C rods. The volume fractions of the B_4C, coolant, and structure (HT9) of the B_4C rods are 58.1%, 23.7%, and 18.2%, respectively. The consideration of 8% axial fuel swelling and new B_4C based radial shield assemblies led to a considerable reduction of the initial reactivity due to the reduction of fuel density and the neutron absorption by B_4C radial shield assemblies. To compensate this reduction of core reactivity, the central GEMs were replaced with the lead reflectors, and the active fuel length of the outer core was increased by 10 cm in the final core. In addition, the SSFZ (Special Sodium Flowing Zone) was suggested to replace the GEMS in the outer reflector region to further reduce sodium void worth. In the SSFZ, the cross flow of sodium coolant from the fuel assemblies facing them is allowed, which increases the neutron leakage under sodium coolant voiding. Also, the holes on the ducts of the fuel assemblies facing SSFZ should be considered to allow the sodium coolant to flow into SSFZ but we did not consider these holes in our neutronic analysis. But it should be addressed that these SSFZs can have several issues related to the coolant flowing path, which should be analyzed in the future.

Fig. 8 shows the radial and axial configurations of the final core (i.e., Design II core). Fig. 9 compares the changes of k_{eff} values as depletion for the Design I–B and Design II cores (i.e., final core). As shown in Fig. 9, the cycle length of the final core is considerably reduced to 54 EFPYs compared to the Design I–B core.

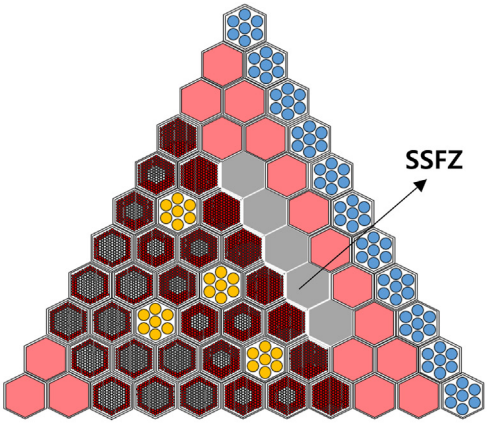

(a) Radial configuration

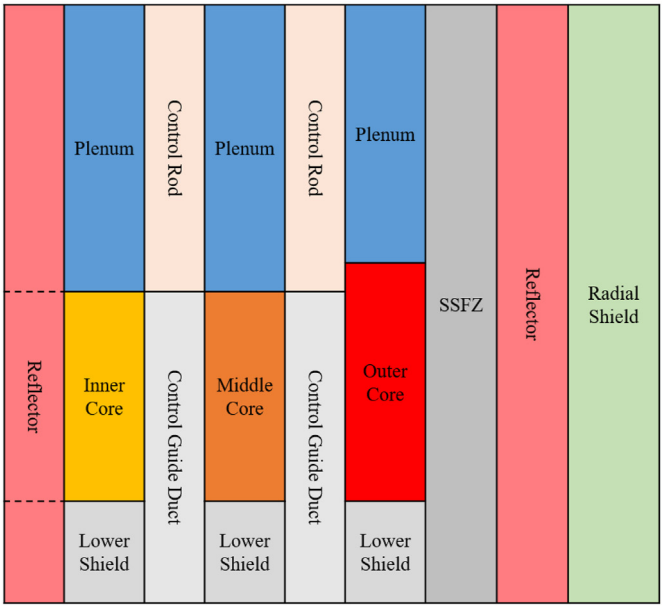

(b) Axial configuration

Fig. 8. Fig. 8. Radial and axial configuration of Final core.

Table 4 compares the performances of the Design I–B and the final cores. As shown in Table 4, the final core has a much smaller burnup reactivity swing of 618 pcm (<1$ with β_{eff} at BOC) but lower average burnup by 15% due to its shorter cycle length of 54 EFPYs than the Design I–B core. The final core has a lower sodium void worth by 283 pcm only for active core sodium voiding than the Design I–B core and it has nearly zero sodium void worth of 35 pcm (i.e., 0.08$) with additional sodium voiding for sodium plenum and SSFZ at EOC. The lower plutonium and TRU contents in the blanket fuels of the final core are due to its lower burnup.

3.3. Quasi-static reactivity balance analysis

Finally, the quasi-static reactivity balance analysis developed by Wade and Hill [23] was performed using the reactivity coefficients given in Table 5 to check the inherent safety under unprotected accidents such as ULOF (unprotected loss-of-flow), ULOHS (unprotected loss-of-heat-sink), and UTOP (unprotected transient-overpower). In this work, the inherent safety means that a

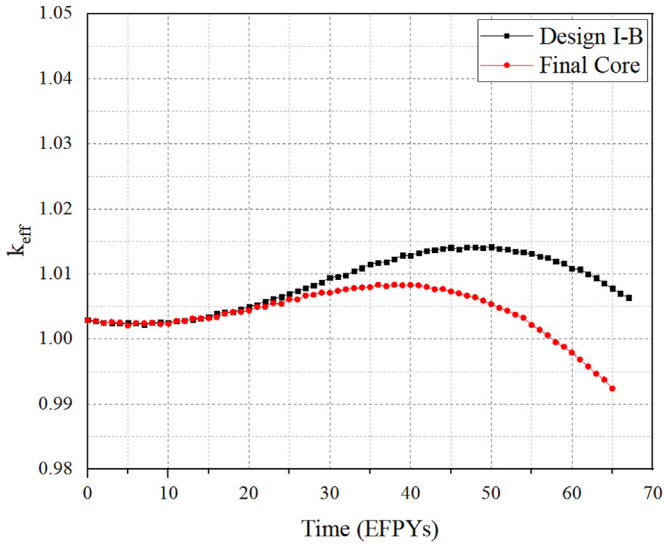

Fig. 9. Comparison of evolutions of k_{eff} for Design I–B and Final core.

reactor leads to a passive safe shutdown state only through the reactivity feedback effects (e.g., Doppler effect, fuel axial expansion, radial expansion of core support plate and so on) without exceeding the limits ensuring core integrity. From Wade and Hill [23], it was shown that the inherent safety for a sodium-cooled fast reactor using metallic fuel is satisfied if the following conditions are met:

$$\begin{aligned} A &= (\alpha_D + \alpha_e)\Delta T_f < 0, \\ B &= (\alpha_D + \alpha_e + \alpha_{co} + 2\alpha_{RD} + 2\alpha_R)\Delta T_C/2 < 0, \\ C &= \alpha_D + \alpha_e + \alpha_{co} + \alpha_R < 0, \end{aligned} \tag{1}$$

And

$$\begin{aligned} &A/B \le 1 \text{ for ULOF}, \\ &1 \le \frac{C\Delta T_C}{B} \le 2 \text{ for ULOHS}, \\ &\frac{\Delta\rho_{Top}}{B} \le 1 \text{ for UTOP}. \end{aligned} \tag{2}$$

In Eq. (1), the reactivity coefficients α_D, α_e, α_{co}, α_{RD}, and α_R represent the temperature reactivity coefficients by Doppler, fuel axial expansion, coolant expansion, control rod driveline expansion, and core radial expansion, respectively. ΔT_f and ΔT_C represent the incremental fuel temperature increase, and the coolant temperature rises under full power condition, respectively. In this work, we assumed the typical values of 150 and 155 °C for these temperature rises in sodium-cooled fast reactors. $\Delta\rho_{Top}$ represents the maximum reactivity insertion due to a control rod runout, which is related to the burnup reactivity swing. This analysis was conservatively performed with the reactivity coefficients at EOC but burnup reactivity swing is considered for UTOP because it is the most conservative condition.

The results of the quasi-static reactivity balance analysis for the Design I, Design I-A, Design I–B, and the final cores are summarized in Table 5. Table 5 shows that the Design I-A, Design I–B, and the final cores satisfy all the conditions while the Design I core does not satisfy the fifth condition which is associated with ULOHS due to its less negative reactivity coefficients by fuel axial and coolant expansions. In particular, it is noted that the Design I–B and the final cores satisfy all the conditions with the large margins and that the

Table 4
Comparison of the main performances of the Final core.

Parameters	Design I–B	Final core
Cycle length (EFPYs)	67	54
Burnup reactivity swing (pcm)	1181	618
Initial U^{235} enrichment (wt%) for driver fuel		
Inner/Middle/Outer	15.32/15.32/15.32	16.7/16.7/15.51
Actinide inventories (kg, driver/blanket)	29,132/10,419	26,802/9586
Fuel burnup (MWd/kg)		
Inner core (driver/blanket)	184/98	169/80
Middle core (driver/blanket)	175/91	134/69
Outer core (driver)	139	108
Total core	144	123
Sodium void worth (pcm, BOC/EOC)		
Active core	365/2000	393/1717
Active core + sodium plenum	−948/883	−951/599
Active core + sodium plenum + SSFZ	NA	−1029/35
Reactivity coefficients (pcm/K, BOC/EOC)		
Doppler coefficient	−0.436/−0.449	−0.456/−0.319
Fuel axial expansion	−0.281/−0.323	−0.257/−0.398
Core support radial expansion	−0.852/−1.139	−0.815/−1.152
Coolant expansion	−0.4721/0.3603	−0.4806/0.3329
Effective delayed neutron fraction (β_{eff})	0.00665/0.00414	0.00733/0.00450
Pu content in driver fuel (wt%, EOC)		
Inner/middle/outer	9.09/8.55/7.08	6.81/6.50/5.80
Pu content in blanket fuel (wt%, EOC)		
Inner/middle/outer	9.34/8.85/0	7.84/7.53/0
TRU content in driver fuel (wt%, EOC)		
Inner/middle/outer	9.51/8.92/7.36	7.12/6.78/6.01
TRU content in blanket fuel (wt%, EOC)		
Inner/middle/outer	9.46/8.97/0	7.94/7.62/0

Note: All values in this table are calculated with Serpent.

Table 5
Results of the quasi-static reactivity balance analysis.

Parameters	Design I	Design I-A	Design I–B	Final core
A (pcm)	−70.0	−79.4	−115.8	−107.6
B (pcm)	−179.3	−178.3	−208.4	−208.3
C (pcm/°C)	−1.131	−1.159	−1.550	−1.536
A/B	0.391	0.445	0.555	0.516
$C\Delta T_c/B$	0.9779	1.008	1.153	1.143
$\rho_{ex}/\lvert B\rvert$	0.5667	0.569	0.348	0.112

final core satisfies the last condition associated with UTOP with the largest margin due to its smallest burnup reactivity swing.

The fuel pin-wise power distributions (W) of the final core at 0, 27, and 54 EFPYs are compared in Fig. 10. As in the cores considered in the initial scoping analysis, fission powers at BOC are mainly generated in the driver fuels of middle and outer cores, and then fission power propagates into driver rods and partially into blanket rods of the inner core. Also, from this figure, it is shown that the fuel rod-wise linear power density is less than ~150 W/cm, and it is considered that the maximum linear power density would be less than ~200 W/cm with the conservatively high axial power peaking factor of 1.3.

4. Summary and conclusion

In this work, new small sodium cooled fast reactor cores that can be operated without refueling over ultra-long-cycle of 54–76 EFPYs were designed and analyzed. In particular, new cores do not only use the usual homogeneous fuel assemblies but also many heterogeneous ones comprised of driver and blanket fuel rods to allow the power shifting within the fuel assemblies. In each heterogeneous fuel assembly, the driver fuels are located in the outer region enclosing blanket rods to enhance breeding and core reactivity by making the driver fuel rods facing together. The neutronic characteristics of the cores were evaluated using high fidelity heterogeneous Monte Carlo calculations with MCNP6 and Serpent to reflect the detailed heterogeneities of the new fuel assemblies. A reference core was designed such that it has ultra-long-cycle of 76 EFPYs, leading to high burnup and small burnup reactivity swing of 1590 pcm. A power distribution analysis of this core showed that the power distribution well spreads out through the core by allowing the power shifting within fuel assemblies as fuel depletion. However, this core has considerable positive sodium void worth at EOC in spite of its negative sodium void worth at BOC. In particular, the sodium void worth for coolant voiding only in the active core is quite high up to ~2171 pcm at EOC.

To reduce the sodium void worth, we employed the introduction of the upper sodium plenum above active fuel. The sodium voiding, including the upper sodium plenum, significantly reduces smaller sodium void worth by 1046–1117 pcm at EOC. It was shown that the GEMs inserts negative reactivity by ~430 pcm under loss of the primary coolant flow at EOC.

The final core was designed by considering the axial fuel swelling and realistic radial shield assemblies using B_4C rods, which led to a considerable reactivity decrease. To compensate for this reactivity decrease, the GEMs in the central core region were replaced with lead reflector assemblies, and the active fuel length of the outer core was increased by 10 cm. In addition, SSFZ replaced the GEMs in the outer reflector region to reduce the sodium void worth by enhancing radial neutron leakage under sodium coolant voiding. It was shown that the final core has nearly zero sodium void worth of ~35 pcm even at EOC, a very low burnup reactivity swing of 618 pcm over its cycle length of 54 EFPYs, and high average burnup of 123 MWd/kg. The results of the quasi-static reactivity balance analysis showed that the final core satisfies all the conditions for inherent safety with large margins due to its excellent temperature reactivity coefficients. However, it should be noted

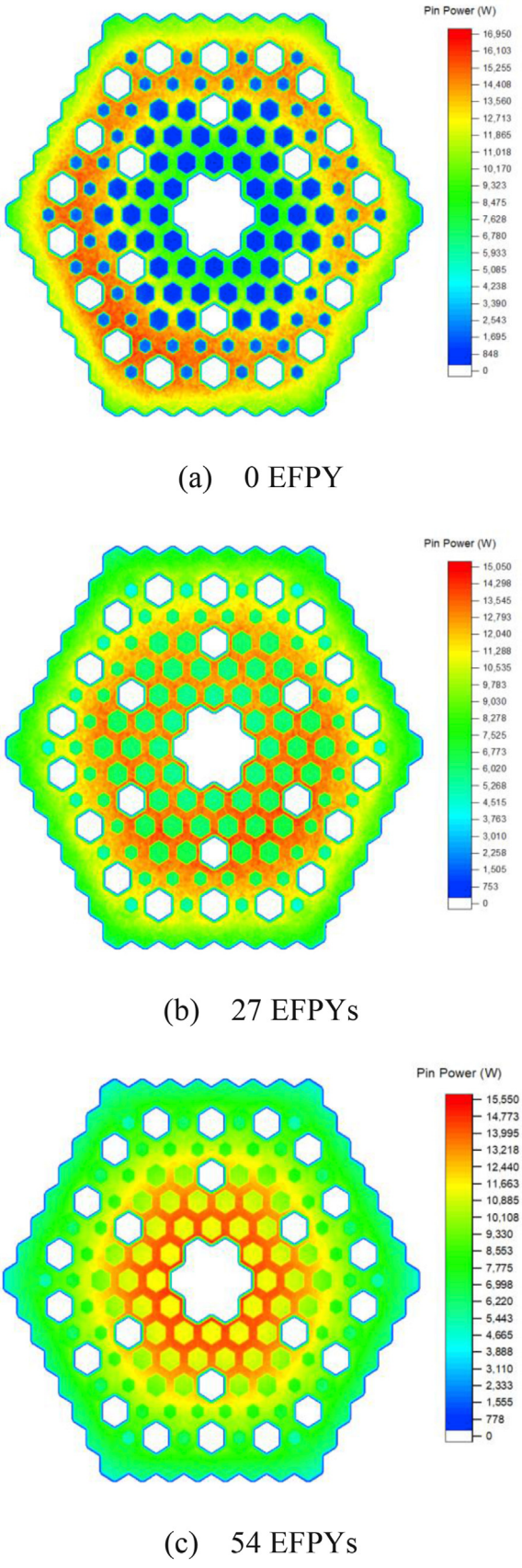

Fig. 10. Comparison of the power distributions at different depletion times of the Final core.

again that the use of the upper sodium plenum region requires a ventilation pass of fission gas, which is a key element for achieving the nearly zero sodium void worth.

Declaration of competing interest

The authors declare that they have no known competing financial interests or personal relationships that could have appeared to influence the work reported in this paper.

Acknowledgements

This work was supported by the Basic Science Research Program through the National Research Foundation of Korea (NRF) funded by the Ministry of Education, Science, and Technology (Grant No. NRF-2015R1D1A1A02061941).

References

[1] A.J. Kuperman, Plutonium for Energy ? – Explaining the Global Decline of MOX, The University of Texas at Austin, October 2018.
[2] K. Tucek, J. Carlsson, H. Wider, Comparison of sodium and lead-cooled fast reactors regarding reactor physics aspects, severe safety and economical issues, Nucl. Eng. Des. 236 (2006) 1589–1598.
[3] W.S. Yang, Fast reactor physics and computational methods, Nucl. Eng. Technol. 44 (2012) 177–198.
[4] T.K. Kim, T.A. Taiwo, Fuel Cycle Analysis of Once-Through Nuclear Systems : Fuel Cycle Research & Development, ANL-FCRD-308, Lemont, Illinois, US, 2010.
[5] W. You, S.G. Hong, A core physics study of advanced sodium-cooled TRU burners with thorium- and uranium-based metallic fuels, Nucl. Technol. 194 (2016) 217–232.
[6] OECD/NEA, Minor Actinide Burning in Thermal Reactors, A Report by the Working Party on Scientific Issues of Reactor Systems, 2013.
[7] T.A. Taiwo, T.K. Kim, J.A. Stillman, R.N. Hill, M. Salvatores, P.J. Finck, Nucl. Technol. 155 (2006) 34–54.
[8] H. Sekimoto, K. Ryu, Y. Yoshimura, CANDLE: the new burnup strategy, Nucl. Sci. Eng. 130 (2001) 306–317.
[9] H. Sekimoto, A. Nagata, Performance optimization of the CANDLE reactor for nuclear energy sustainability, Energy Convers. Manag. 51 (2010) 1788–1791.
[10] C. Ahlfeld, et al., Conceptual design of a 500MWe travelling wave demonstration reactor plant, in: Proceedings of ICAPP 2011, 2011. Nice, France, May 2-5.
[11] J. Gilleland, J. Petrosski, K. Weaver, The traveling wave reactor: design and development, Engineering 2 (2016) 88–96.
[12] E. Greenspan, A phased development of breed-and-burn reactors for enhanced nuclear energy sustainability, Sustainability 4 (2012) 2745–2764.
[13] S.G. Hong, H.L. Hyun, W. You, Core design options of an ultra-long-cycle sodium cooled reactor with effective use of PWR spent fuel for sustainable energy supply, Int. J. Energy Res. 41 (2017) 854–866.
[14] S.G. Hong, J.H. Kim, W. You, A neutronic design study of lead-bismuth-cooled small and safe ultra-long-life cores, Ann. Nucl. Energy 85 (2015) 58–67.
[15] D. Hartanto, C. Kim, Y. Kim, An optimization study on the excess reactivity in a linear breed-and-burn fast reactor (B&BR), Ann. Nucl. Energy 94 (2016) 62–71.
[16] M.J. Driscoll, B. Atefi, D.D. Lanning, An Evaluation of the Breed/burn Fast Reactor Concept, MIT report MITNE-229. MIT, Cambridge, MA, USA, 1979.
[17] P. Hejzlar, R. Ptroski, et al., LLC Traveling wave reactor development overview, Nucl. Eng. Technol. 45 (2013) 731–744.
[18] K.J. Choi, Y. Jo, S.G. Hong, A neutronic design study of small ultra-long-life SFR core using serpent heterogeneous Monte Carlo calculation, San Francisco, CA, in: Proceedings of the Pacific Basin Nuclear Conference (PBNC) 2018, 2018. September 30 – October 4.
[19] G. Jung, W. You, S.G. Hong, A preliminary design study of ultra-long-life SFR cores having heterogeneous fuel assemblies, Gyeongju, Korea, in: Proceedings of the KNS 2016 Autumn Meeting, 2016. Oct 26-28.
[20] G. Jung, Y. Jo, S.G. Hong, Alternative design options for small ultra-long-life sodium cooled fast reactor core using heterogeneous assemblies, in: Proceedings of the PHYSOR 2018, Cancun, Mexico, 2018. April 22-26.
[21] D.B. Pelowitz, MCNP6™ User's Manual Version 1.0. LA-CP-13-00634, 2013. Rev.0.
[22] J. Leppanen, M. Pusa, T. Viitanen, V. Valtavirta, T. Kaltiaisenaho, The serpent Monte Carlo code : status, development and applications in 2013, Ann. Nucl. Energy 82 (2015) 142–150.
[23] D.C. Wade, R.N. Hill, The design nationale of the IFR, Prog. Nucl. Engergy 31 (1997) 13–42.
[24] K. Sun, et al., A neutronics study for improving the safety and performance parameters of a 3600 MWth sodium-cooled fast reactor, Ann. Nucl. Energy 53 (2013) 464–475.

[25] S.G. Hong, E. Greenspan, Y.I. Kim, The encapsulated nuclear heat source (ENHS) reactor core design, Nucl. Technol. 149 (2005) 22–46.
[26] T. Tak, J. Choe, Y. Jeong, D. Lee, T.K. Kim, S.G. Hong, Feasibility study on ultra-long cycle operation and material performance for compact liquid metal-cooled fast reactors : a review work, Int. J. Energy Res. 39 (2015) 1859–1878.
[27] N.E. Stauff, T.K. Kim, D. Yun, T.A. Taiwo, H.S. Khalil, Application of an annular metallic fuel with lower gas plenum for sodium-cooled fast reactor, Trans. Am. Nucl. Soc. 108 (2013) 747–749.
[28] M.S. Chenaud, N. Devictor, et al., Status of the ASTRID core at the end of the pre-conceptual design phase 1, Nucl. Eng. Technol. 45 (2013) 721–730.
[29] P. Sciora, et al., Low void effect core design applied on 2400 MWth SFR reactor, Nice, France, in: Proceedings of ICAPP 2011, 2011. May 2-5.